



Cite this: DOI: 10.1039/c5cy01371b

Highly monodisperse Pt(0)@AC NPs as highly efficient and reusable catalysts: the effect of the surfactant on their catalytic activities in room temperature dehydrocoupling of DMAB†

Betül Çelik,‡ Esmâ Erken,‡ Sinan Eriş, Yunus Yıldız, Birgütay Şahin, Handan Pamuk and Fatih Sen*

Addressed herein, we report the development of highly efficient and monodisperse Pt(0) nanoclusters for the dehydrocoupling of dimethylamine–borane (DMAB) which is considered to be one of the new hydrogen storage materials. The prepared Pt(0) nanoclusters were *in situ* generated for the first time from the reduction of PtCl₄ and use of dipentylamine (DPA) and tripentylamine (TPA) ligands on activated carbon for the dehydrocoupling of dimethylamine–borane at room temperature and characterized by ICP-OES, XRD, TEM, HR-TEM, AFM, EDX, and XPS techniques. All the results show that highly crystalline and stable colloidal Pt(0)/DPA@AC and Pt(0)/TPA@AC nanoparticles have been formed and Pt(0)/DPA@AC and Pt(0)/TPA@AC were found to be two of the most active and long-lived catalysts with superior reusability performance in the dehydrocoupling of DMAB at room temperature.

Received 20th August 2015,
Accepted 8th October 2015

DOI: 10.1039/c5cy01371b

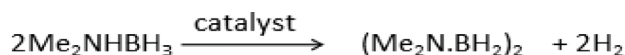
www.rsc.org/catalysis

Introduction

Energy is mostly supplied by the combustion of fossil fuels which emits large amounts of greenhouse gases, thus causing global warming.¹ On the way towards a sustainable energy future,² hydrogen appears to be the best energy carrier.^{3,4} However, the safe and efficient storage of hydrogen is still one of the most important and challenging problems in hydrogen economy.⁵ For the past decades, there has been rapidly growing interest in searching for suitable hydrogen storage materials on the way towards a sustainable energy future.^{2–5} Among the various kinds of solid hydrogen storage materials,^{6–10} dimethylamine–boranes (DMABs) appear to be one of the most promising solid hydrogen carrier materials.^{11,12} DMAB has various advantages: it is nontoxic, it exists as a crystalline solid at room temperature, is stable in air and water, and is environmentally friendly. Of particular interest, recent studies have already shown that DMAB is really a model substrate since the products are relatively easy to attain compared to the other ammonia boranes (Scheme 1).

Further, various homogeneous and heterogeneous catalysts have been tested for dehydrocoupling of DMAB such as

Ru, Rh, Pd, and Ir complexes,¹³ Ru(H)(PMe₃)(PNP) and *trans*-Ru(H)₂(PMe₃)(PNP^H),¹⁴ [Rh(1,5-cod)(μ-Cl)]₂,^{15–17} [Cp₂Ti],^{18,19} [RuH₂(η²-H₂)₂(PCy₃)₂] and [RuH₂(η²:η²-H₂B-N(Me)₂(PCy₃)₂),²⁰ RhCl₃, colloidal Rh/[Oct₄N]Cl and Rh/Al₂O₃,¹⁵ laurate-stabilized Rh(0),²¹ hexanoate-stabilized Rh(0),²² aminopropyltriethoxysilane-stabilized Ru(0),²³ Re complexes,²⁴ Rh_{4–6} clusters,²⁵ RhCl(PHCy₂)₃,²⁶ Ru/ZIF-8,² [Ru(*p*-cym)(bipy)Cl]Cl,²⁷ Pd(0)/MOF,²⁸ and Pt(0)/amylamine.²⁹ Although the record activity has been achieved by using the homogeneous [η⁵C₅H₃-1,3(SiMe₃)₂]₂Ti₂ catalyst,³⁰ the current research has focused on the development of new metal nanoparticle catalysts because of their significant advantages in product isolation, catalyst recovery and reusability.²⁹ We report, for the first time, the preparation and characterization of highly efficient and monodisperse Pt(0) nanoparticles stabilized by the dipentylamine (DPA) and tripentylamine (TBA) ligands on activated carbon, hereafter designated as Pt(0)/DPA@AC and Pt(0)/TPA@AC, respectively. We have also evaluated the effect of the stabilizing ligand on the catalytic activity of room temperature dehydrocoupling of DMAB [(CH₃)₂NHBH₃].



Scheme 1 The catalytic dehydrocoupling of dimethylamine–borane ((CH₃)₂NHBH₃, DMAB).

Sen Research Group, Biochemistry Department, Faculty of Arts and Sciences, Dumlupınar University, Evliya Çelebi Campus, 43100 Kütahya, Turkey.

E-mail: fatih.sen@dupu.edu.tr

† Electronic supplementary information (ESI) available. See DOI: 10.1039/c5cy01371b

‡ These authors equally contributed to this work.

Experimental methods

Reagents and instrumentation

PtCl₄ (99%, Alfa Aesar), tetrahydrofuran (THF) (99.5%, Merck), lithium triethylborohydride (1.0 M dissolved in THF, Sigma Aldrich), dipentylamine and tripentylamine (Sigma Aldrich), and dimethylamine–borane ((CH₃)₂NHBH₃) (Sigma Aldrich) were used as received from suppliers. THF was distilled over sodium under an argon atmosphere and stored under an inert atmosphere. De-ionized water was filtered by a Millipore analytical grade water purification system (18 MΩ). All glassware and Teflon-coated magnetic stir bars were cleaned with aqua regia, followed by washing with distilled water before drying.

TEM samples were prepared by dropping of a 0.5 mg mL⁻¹ ethanol solution of the prepared catalysts with an activated carbon support on a carbon covered 400-mesh copper grid, and then the solvent was vaporized. Elimination of excess solution was performed with adsorbent paper and the sample was dried under vacuum at room temperature before analysis. TEM analysis was carried out by using a JEOL microscope operated at 200 kV. More than 300 particles were calculated to get the integrated information about the overall distribution of a Pt-based catalyst sample.

During X-ray Photoelectron Spectroscopy (XPS) analysis, a Specs spectrometer was employed and an X-ray source for the Kα lines of Mg (1253.6 eV, 10 mA) was used. Sample preparation was done by depositing the catalyst on Cu double-sided tape (3 M Inc.). The C 1s line at 284.6 eV was selected as a reference point and all the XPS peaks were fitted using a Gaussian function and the C 1s line at 284.6 eV was used as the reference line.

XRD analysis was performed using a PANalytical Empyrean diffractometer with an Ultima+theta-theta high resolution goniometer, having an X-ray generator (Cu Kα radiation, $k = 1.54056 \text{ \AA}$) and operating conditions of 40 kV and 40 mA.

In order to examine the quantity of platinum in each catalyst, a Leeman Lab Inductively Coupled Plasma spectrometer (ICP) was used.

With the aim of enlightening the surface topographies of the prepared catalysts, the AFM technique was used with the sample at ambient temperature using a Park Systems AFM XE-100E operated in the intermittent contact (“tapping”) mode. We used 0.01–0.025 ohm cm antimony-doped silicon AFM probes (Ultrasharp TESP) having cantilever spring constants of 20–80 N m⁻¹ and resonance frequencies of 328–379 kHz. The tip radius of curvature is approximately 2 nm. For this examination, first, a sample for AFM analysis was prepared by diluting the product solutions by 300-fold or more with DI water and placing 2.5 μL of the final solution directly onto the freshly cleaved mica disk (ESI[†]) and the solution was dried under vacuum at room temperature for at least 12 h.

The ¹¹B NMR spectra were recorded on a Bruker Avance DPX 400 MHz spectrometer (128.2 MHz for ¹¹B NMR).

The *in situ* preparation of Pt(0)/DPA@AC and Pt(0)/TPA@AC and their catalytic activities in the dehydrocoupling of DMAB

Prior to starting the catalytic activity measurements of Pt(0)/DPA@AC and Pt(0)/TPA@AC used in the dehydrocoupling of

DMAB, a typical jacketed, three-necked reaction flask was connected to a water filled cylinder glass tube under a dry nitrogen atmosphere. In order to eliminate existing oxygen and water prior to all catalytic tests, the jacketed reaction flask was kept under vacuum for at least 15 min, and then nitrogen gas was allowed to occupy it. The measurement of the quantity of hydrogen evolution during the dehydrocoupling of DMAB was performed so as to examine the catalytic activity of the prepared nanoparticles. After the mixing of 0.25 mmol (0.081 g) of PtCl₄ dissolved in a small amount of anhydrous tetrahydrofuran and 0.25 mmol of DPA or TPA ligand, 1.0 mmol of DMAB in a small amount of THF was added into the jacketed reaction flask thermostated at 25.0 ± 0.1 °C, and then hydrogen liberation was started. In order to observe hydrogen gas generation from the catalytic reaction solution, a typical water-filled gas burette system was used and the water displacement was recorded. After completion of the catalytic test, an approximately 0.5 mL aliquot of the reaction solution in the reactor was taken using a glass Pasteur pipet and added to 1 g of CDCl₃ in a quartz NMR sample tube.

Reusability performance of Pt(0)/DPA@AC and Pt(0)/TPA@AC in the dehydrocoupling of DMAB

After the first catalytic reaction of the dehydrocoupling of 1.0 mmol of DMAB starting with Pt(0)/DPA@AC and Pt(0)/TPA@AC, the reaction flask was disassembled from the line and attached to a vacuum line. After the vaporization of the volatiles, the solid residue was weighed and used again in the dehydrocoupling reaction under the same conditions (in a small amount of THF at 25.0 ± 0.1 °C). This procedure was followed until four catalytic runs were performed.

Mercury (Hg(0)) poisoning of Pt(0)/DPA@AC and Pt(0)/TPA@AC in the dehydrocoupling of DMAB

Elemental Hg (300 equiv.) was placed into a small amount of THF solution containing Pt(0)/DPA@AC and Pt(0)/TPA@AC in the jacketed, three-necked reaction flask. After 4 hours of stirring, this solution was used in the dehydrocoupling of 1.0 mmol of DMAB under the identical situations reported above.

Results and discussion

Characterization of Pt(0)/DPA@AC and Pt(0)/TPA@AC

Easy reproductions of the prepared nanoparticles were carried out by *in situ* techniques using anhydrous THF solutions of the DPA and TPA ligands at room temperature. Without any ligand like DPA and TPA used for stabilization, sudden agglomeration and precipitation out of the THF solution of the prepared Pt(0) nanoparticles were monitored. This demonstrated that the DPA and TPA ligands are highly efficient stabilizing agents for the platinum(0) nanoparticles. Pt(0)/DPA@AC and Pt(0)/TPA@AC were isolated successfully by

washing with dry ethanol to eliminate excess ligand and vaporizing the solvent under vacuum atmosphere.

The highly efficient and monodisperse Pt(0)/DPA@AC and Pt(0)/TPA@AC nanoparticles were characterized by ICP-OES, XRD, TEM, HRTEM, AFM and XPS. Spectroscopic studies and applications of the catalysts were carried out by hydrogen gas production tests for the dehydrocoupling of DMAB.

The X-ray diffraction patterns of the highly monodisperse Pt(0)/DPA@AC and Pt(0)/TPA@AC are illustrated in Fig. 1 and indicate that all the diffraction patterns have similar peaks at around $2\theta = 39.90, 46.60, 67.50, 81.52, 86.03$ and $2\theta = 39.68, 46.15, 67.32, 81.07, 89.90$, respectively. These peaks are planes of the face-centered cubic (fcc) crystal lattice of platinum (JCPDS-ICDD, card no. 04-802) that are due to Pt (111), (200), (220), (311), and (320) for Pt(0)/DPA@AC and Pt(0)/TPA@AC. In order to find the lattice parameter (a_{Pt}) values and average crystallite sizes of the metal particles, the Pt (220) diffraction peak of the prepared catalysts has been used. The lattice constant values have been calculated to be 3.922 and 3.931 Å for Pt(0)/DPA@AC and Pt(0)/TPA@AC, respectively, which are very close to the 3.923 Å obtained by the following equation for pure Pt.^{31a-e}

$$\sin \theta = \frac{\lambda \sqrt{h^2 + k^2 + l^2}}{2a} \quad (\text{for a cubic structure})$$

Furthermore, the average crystallite particle sizes of the highly monodisperse Pt(0)/DPA@AC and Pt(0)/TPA@AC were calculated to be 3.30 ± 0.35 nm and 3.77 ± 0.39 nm, respectively, by the use of the following formula:³²

$$d(\text{\AA}) = \frac{k\lambda}{\beta \cos \theta}$$

where k = a coefficient (0.9); λ = the wavelength of X-ray used (1.54056 Å), β = the full width at half-maximum of respective diffraction peak (rad), and θ = the angle at the position of peak maximum (rad).

The high resolution electron micrograph (HRTEM) and particle size histogram of Pt(0)/DPA@AC and Pt(0)/TPA@AC show the highly monodisperse morphology of the catalysts as

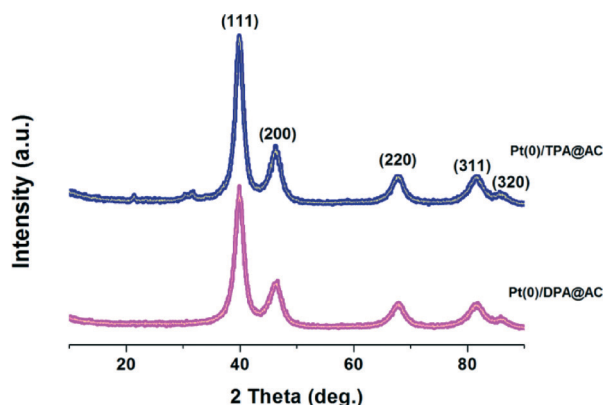


Fig. 1 XRD of Pt(0)/DPA@AC and Pt(0)/TPA@AC.

indicated in Fig. 2. The average particle sizes of Pt(0)/DPA@AC and Pt(0)/TPA@AC were found to be 3.48 ± 0.39 nm and 3.86 ± 0.43 nm and a uniform distribution of the catalyst particles with a very narrow range on activated carbon was detected. The HRTEM results also revealed that most of the particles were in a spherical shape, and no agglomerations were observed in the prepared catalysts. Moreover, the representative atomic lattice fringes obtained by HRTEM for Pt(0)/TPA@AC are shown in Fig. 2, and it is found that the Pt (111) and (200) plane spacing values are 0.228 and 0.196 nm on the prepared catalysts, respectively, which are very close to the nominal Pt (111) and (200) spacing values of 0.227 and 0.198 nm, respectively.^{33a-d}

The investigation of the height diameter distribution, as shown in Fig. S1,[†] was also carried out by Atomic Force Microscopy (AFM). It was shown that the AFM particle height distributions are in very good agreement with the particle size obtained by XRD and TEM.

For the determination of the effect of the oxidation state of platinum on the catalytic activities for the prepared catalysts, the Pt 4f region has been evaluated by using X-ray photoelectron spectroscopy (XPS). Shirley's method was used to subtract the background, then the Gaussian-Lorentzian method was utilized for fitting of all the XPS peaks and all the peaks were investigated in terms of the relative peak area and chemical shifts of Pt. The estimation of the relative intensity of the species was performed by calculating the integral of each peak, after smoothing and subtracting of the Shirley-shaped background. In the XPS spectrum, accurate binding energies (± 0.3 eV) were examined by referencing to the C 1s peak at 284.6 eV. It was seen that the Pt 4f photoelectron spectra for the prepared catalysts consist of two pairs of doublets as shown in Fig. 3. For both catalysts, the most intense doublet at about 71.0 and 74.3 eV is the indication of metallic platinum^{31a,32,34-38} and the other doublet at about 73.9 and 77.4 eV is most probably caused by a very small fraction of the oxidized Pt⁴⁺ species possibly because of the

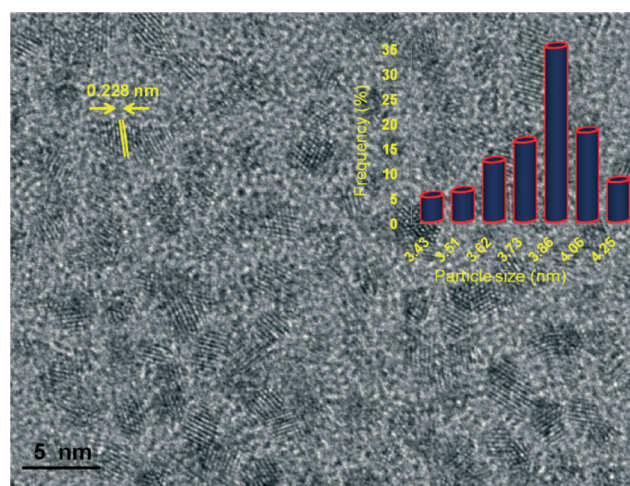


Fig. 2 High resolution transition electron micrograph and particle size histogram of the Pt(0)/TPA@AC catalyst.

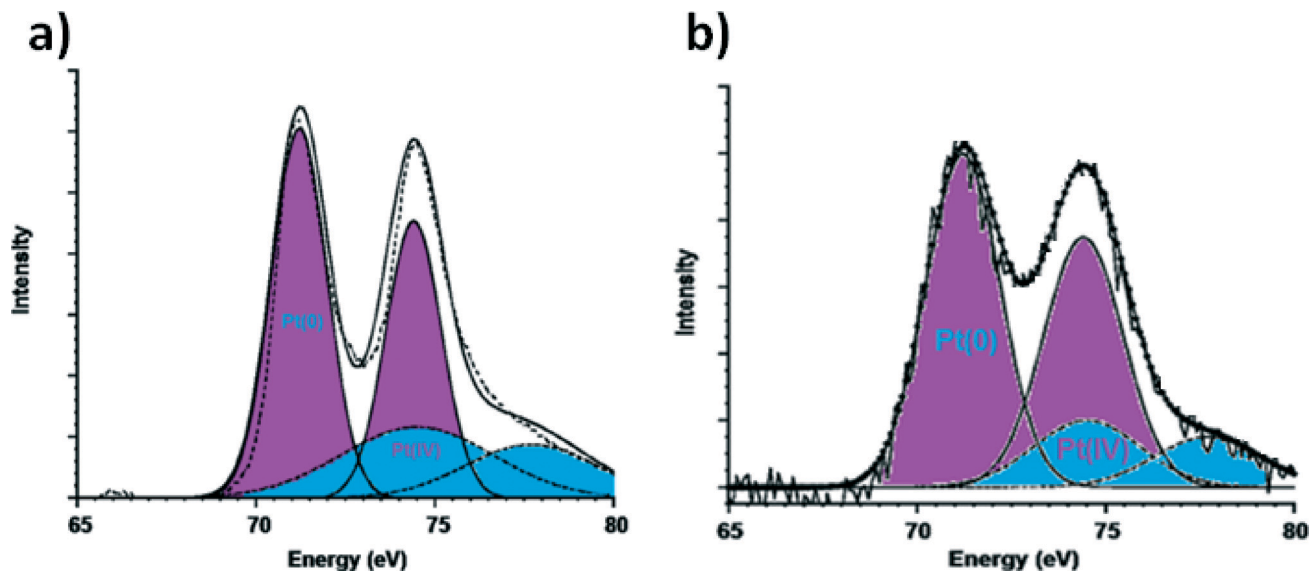


Fig. 3 Pt 4f electron spectra of Pt(0)/DPA@AC (a) and Pt(0)/TPA@AC (b).

unreduced Pt precursor or PtO_x species produced when the catalyst was in contact with the atmosphere, as tabulated in Table 1.

Catalytic activity of Pt(0)/DPA@AC and Pt(0)/TPA@AC in the dehydrocoupling of dimethylamine–borane (DMAB)

In the catalytic dehydrocoupling of DMAB at 25 ± 0.1 °C, Pt(0)/DPA@AC and Pt(0)/TPA@AC were used as catalysts and their catalytic activities were investigated by the measurement of the volume of hydrogen evolution during the reaction and the determination of the reaction products was carried out by ^{11}B NMR spectroscopy. After the addition of DMAB into a THF solution of Pt(0)/DPA@AC and Pt(0)/TPA@AC, the hydrogen evolution begins quickly with initial turnover frequencies of 32.86 h^{-1} and 34.14 h^{-1} , which go on up until 1 equivalent of H_2 per mol DMAB is emitted. Only ~8–10% conversion is observed after the induction time period (10 min), when PtCl_4 is used as a pre-catalyst under the same conditions in the dehydrocoupling of DMAB as shown in Fig. S2.† At the end of the reaction, the combination of Pt nanoparticles and their precipitation out of the solution were observed within 10 min by naked eye due to the weakly coordinating chloride anion of PtCl_4 which cannot yield enough stabilization for the platinum(0) nanoparticles.³⁹ NMR data proves the complete conversion of $(\text{CH}_3)_2\text{NHBH}_3$ ($\delta = \sim 12.7$ ppm) to $[(\text{CH}_3)_2\text{NBH}_2]_2$ ($\delta = \sim 5$ ppm)

which shows the dehydrocoupling reaction of DMAB (at 1.0 equiv. H_2 generation) even at room temperature. In addition, in order to identify the heterogeneous nature of Pt(0)/DPA@AC and Pt(0)/TPA@AC in the dehydrocoupling of DMAB, the mercury poisoning experiment was performed and the results show that the reaction is completely eased after the addition of 300 equiv. of $\text{Hg}(0)$ per Pt and that Pt(0)/DPA@AC and Pt(0)/TPA@AC act as heterogeneous catalysts.

Determination of the activation parameters (E_a , ΔH^\ddagger , and ΔS^\ddagger) for Pt(0)/DPA@AC and Pt(0)/TPA@AC catalyzed dehydrocoupling of DMAB

The stoichiometric ratio of generated H_2 to $(\text{CH}_3)_2\text{NHBH}_3$ versus time was plotted for the catalytic dehydrocoupling of DMAB starting with highly monodisperse Pt(0)/DPA@AC and Pt(0)/TPA@AC at four different temperatures as shown in Fig. 4. It was monitored that the catalytic dehydrocoupling rate of DMAB was temperature dependent.

Additionally, even at a low temperature (20 °C), the dehydrocoupling of DMAB can be catalysed by Pt(0)/DPA@AC and Pt(0)/TPA@AC, producing 1.0 equiv. of H_2 . The rate constants (k_{obs}) of hydrogen generation from the dehydrocoupling of DMAB were calculated from the linear portions of the plots given in Fig. 5 at four different temperatures in the range of 20–35 °C and were used for the calculation of the activation energy, activation enthalpy and activation entropy from the Arrhenius⁴⁰ and Eyring⁴¹ plots (Table 2).

The activation energy values ($43.31 \text{ kJ mol}^{-1}$ for Pt(0)/TPA@AC and $48.83 \text{ kJ mol}^{-1}$ for Pt(0)/DPA@AC) obtained by the highly monodisperse Pt(0)/DPA@AC and Pt(0)/TPA@AC are not only higher than the Rh(0) nanoparticles (34 kJ mol^{-1}), but also still smaller than the activation energy reported in the literature for the same reaction as tabulated in Table 3. It can be concluded that the highly monodisperse

Table 1 Pt 4f_{7/2} core binding energies, eV, in the prepared catalyst. The numbers in the parentheses are the relative intensities of the species

	Pt 4f _{7/2}		Pt(0)/Pt(IV)
	Pt(0)	Pt(IV)	
Pt(0)/DPA@AC	70.9 (67.0)	73.9 (33.0)	2.03
Pt(0)/TPA@AC	71.0 (74.7)	74.4 (25.3)	2.95

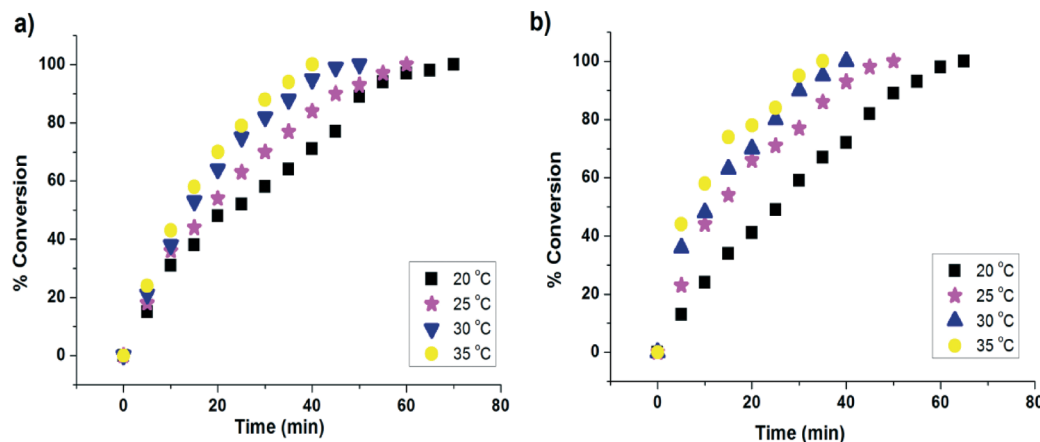


Fig. 4 % Conversion versus time graph for Pt(0)/DPA@AC (a) and Pt(0)/TPA@AC (b) (7.5% mol) catalysed dehydrocoupling of DMAB in THF at various temperatures as given on the plots for Pt(0)/DPA@AC and Pt(0)/TPA@AC.

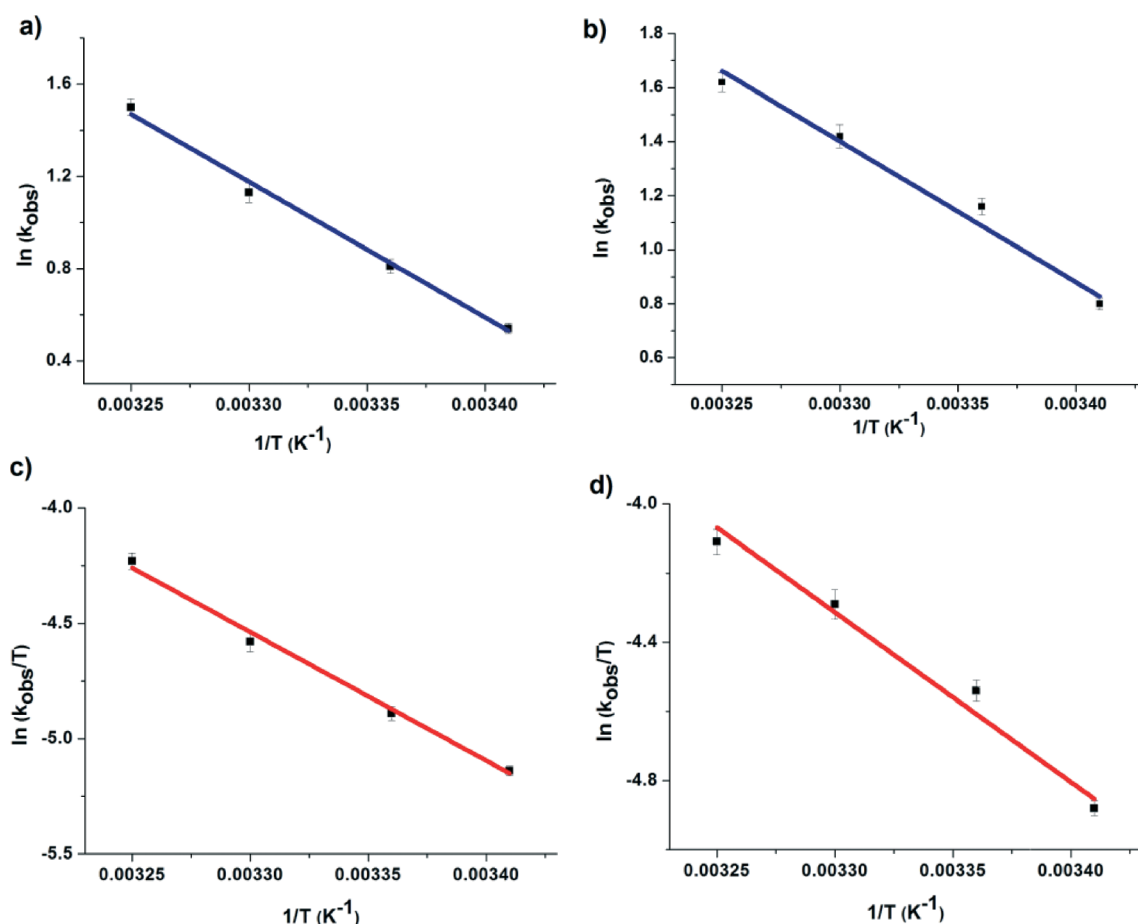


Fig. 5 (a, b) Arrhenius and (c, d) Eyring plots for Pt(0)/DPA@AC (a, c) and Pt(0)/TPA@AC (b, d) catalysed dehydrocoupling of DMAB at various temperatures.

Pt(0)/DPA@AC and Pt(0)/TPA@AC have performed one of the highest catalytic activities for the dehydrocoupling of DMAB reaction. Moreover, it is understood that there is an associative mechanism in the transition state for the catalytic dehydrocoupling of DMAB between the higher negative value

of the activation entropy and the small value of the activation enthalpy. Furthermore, the data indicate that Pt(0)/TPA@AC, which is stabilized by the more branched ligand, TPA, has increased the catalytic activity compared to Pt(0)/DPA@AC most probably due to a higher Pt(0) to Pt(IV) ratio.

Table 2 The activation energy (E_a), activation enthalpy (ΔH^\ddagger), and activation entropy (ΔS^\ddagger) values from the Arrhenius and Eyring plots for Pt(0)/DPA@AC and Pt(0)/TPA@AC

	E_a (kJ mol ⁻¹)	ΔH^\ddagger (kJ mol ⁻¹)	ΔS^\ddagger (J mol ⁻¹ K ⁻¹)
Pt(0)/DPA@AC	48.83	46.31	-115.09
Pt(0)/TPA@AC	43.31	40.79	-98.75

Table 3 Catalysts tested in the dehydrocoupling of DMAB under mild conditions ($\leq 25^\circ\text{C}$)

Entry	(Pre)catalysts	Conv. (%)	TOF	Ref.
1	[RuH(PMe ₃)(NC ₂ H ₄ PPR ₂) ₂]	100	1.5	14
2	[(C ₅ H ₃ -1,3(SiMe ₃) ₂ Ti) ₂]	100	420.0	30
3	[Rh(1,5-cod)(dmpe)]PF ₆	95	1.7	13
4	[Cr(CO) ₅ (η^1 -BH ₃ NMe ₃)]	97	19.9	43
5	<i>trans</i> -PdCl ₂ (P(<i>o</i> -tolyl) ₃) ₂	20	0.2	13
6	<i>trans</i> -RuMe ₂ (PMe ₃) ₄	100	12.4	13
7	[Cp*Rh(<i>m</i> -Cl)Cl] ₂	100	0.9	13
8	Ru(0)/APTS	100	55.0	23
9	(Idipp)CuCl	100	0.3	44
10	Ni(skeletal)	100	3.2	45
11	Rh(0) NPs	100	60.0	22
12	Pt(0)/DPA@AC	100	32.86	This study
13	Pt(0)/TPA@AC	100	34.14	This study
14	Ru(cod)(cot)	40	1.6	23
15	RuCl ₃ ·3H ₂ O	77	2.7	23
16	[Ru(1,5-cod)Cl] ₂ /n	70	2.5	23
17	[Rh(1,5-cod) ₂]OTf	95	12.0	13
18	HRh(CO)(PPh ₃) ₃	5	0.1	13
19	[Ir(1,5-cod) μ -Cl] ₂	95	0.7	13
20	RhCl(PPh ₃) ₃	100	4.3	13
21	Rh(0)/[Oct ₄ N] ⁺ Cl ⁻	90	8.2	13
22	[RhCl(PHCy ₂) ₃]	100	2.6	26
23	[Rh(1,5-cod) μ -Cl] ₂	100	12.5	13
24	RhCl ₃	90	7.9	13
25	Cp ₂ Ti	100	12.3	18
26	[Cr(CO) ₅ (THF)]	97	13.4	43
27	Pd/C	95	2.8	13
28	IrCl ₃	25	0.3	13
29	Pt(0)/BA	100	24.88	46
30	Pt(0)/TBA	100	31.24	46

Furthermore, since the excess of the more branched surfactant, TPA, on the catalyst can easily be removed from Pt(0)/TPA@AC compared to the Pt(0)/DPA@AC, which creates a more active surface area for the dehydrocoupling of DMAB reactions, the catalytic activity of Pt(0)/TPA@AC is higher than that of Pt(0)/DPA@AC.

It has been found that the structure of a surfactant has an effect on the final size of metal nanoparticles; for example, the average particle size of Pt(0)/TPA@AC is larger than that of Pt(0)/DPA@AC. It can be explained that an increase in the particle size might be due to the more branched structure of the TPA compared to the DPA ligand. A more branched surfactant may have a tendency to form a larger hole in the micelles, which in turn would cause an increase in the particle size of the metal which forms in the cavity of the micelle that was confirmed by the AFM, XRD crystallite size, and TEM results.

Reusability performance of Pt(0)/DPA@AC and Pt(0)/TPA@AC in the catalytic dehydrocoupling of DMAB

Pt(0)/DPA@AC and Pt(0)/TPA@AC were also examined in order to find whether the prepared catalysts are isolable and reusable in the dehydrocoupling of DMAB at room temperature. After the completion of the dehydrocoupling of DMAB, highly monodisperse Pt(0)/DPA@AC and Pt(0)/TPA@AC were isolated as black powders, dried under vacuum and then bottled under N₂ atmosphere. The removed catalysts were observed to be still active in the dehydrocoupling of DMAB. Even if at the fourth catalytic run, they maintain >80% of their initial activity (see Fig. S3†). This demonstrates that the prepared platinum nanoparticles are isolable, bottleable, and redispersible yet catalytically active. That is, they can catalyse the dehydrocoupling of DMAB actively several times. The precipitation of the bulk Pt(0) metal may cause the slight decline in catalytic activity in the following runs. This condition can be seen at the end of the 4th catalytic run, in the end forming a clear, colorless (*i.e.*, Pt(0) nanoparticle free) solution by increasing the boron products, which block the active sites.

In fact, the P-XRD pattern of the sample after the 4th catalytic performance reveals that the Pt(0) nanoparticles start to agglomerate.⁴² It is obvious that the initial TOF value of Pt(0)/TPA@AC (34.14 h⁻¹) is higher than the majority of those of the other heterogeneous and homogeneous catalysts listed (see Table 3), except for the previous best heterogeneous (60 h⁻¹)²² and homogeneous³⁰ (420 h⁻¹) catalysts. Except for the Ru(0)/APTS,²³ it is understood that our catalysts are the second best catalyst examples of isolable and reusable nanocatalysts utilized in this substantial catalytic reaction. Most significantly, the reusability performance of our new Pt(0) nanocatalysts is also much better than the previously known most active Rh(0) nanocatalysts which do not have enough stability for isolability and reusability, due to adequate stability of DPA and TPA in our catalyst system, except the Rh(0) nanoparticles.

Conclusions

In conclusion, Pt(0)/DPA@AC and Pt(0)/TPA@AC were reproducibly prepared by the *in situ* optimized reduction method during the catalytic dehydrocoupling of DMAB at room temperature. The characterization of these highly efficient catalysts by using ICP-MS, P-XRD, XPS, TEM, HRTEM and NMR spectroscopy reveals the formation of highly monodisperse Pt(0) nanoparticles. The catalytic performance of both Pt(0)/DPA@AC and Pt(0)/TPA@AC in terms of activity, lifetime and reusability performance was investigated for the catalytic dehydrocoupling of dimethylamine-borane in THF at room temperature. Pt(0)/DPA@AC and Pt(0)/TPA@AC showed unprecedented catalytic activities among all the heterogeneous catalysts tested in the dehydrocoupling of DMAB at room temperature providing initial TOF values of 32.86 h⁻¹ and 34.14 h⁻¹ at complete conversion of DMAB to cyclic diborazane ([Me₂NBH₂)₂) and generation of 1 equiv. of H₂ per

mole of DMAB, respectively. Pt(0)/DPA@AC and Pt(0)/TPA@AC were also found to be highly stable against agglomeration and leaching throughout the catalytic runs in the dehydrocoupling of DMAB, which make them highly reusable and long-lived catalysts. These catalysts almost retain their inherent catalytic activity (80%) even at the fourth catalytic reuse in hydrogen release from dimethylamine–borane. It has been also found that the structure of the surfactant has an effect on the final size and, correspondingly, on the catalytic activities of the metal nanoparticles. The average particle size of Pt(0)/TPA@AC is larger than that of Pt(0)/DPA@AC most probably due to the more branched structure of the TPA compared to the DPA ligand. A more branched surfactant may have a tendency to form a larger hole in the micelles, which in turn would cause an increase in the particle size of the metal which forms in the cavity of the micelle that was confirmed by the AFM, XRD crystallite size, and TEM results. Furthermore, the catalytic activity of Pt(0)/TPA@AC is higher than that of Pt(0)/DPA@AC likely due to the easy isolation of the excess of the more branched surfactant, TPA, on the catalyst compared to the other, which creates a more active surface area for the dehydrocoupling reactions of DMAB. Understanding the existing synergistic effects between the metal and the DPA and TPA ligands remains an active area of research in our group. High catalytic activity, reusability and simple preparation and isolation procedures make Pt(0)/DPA@AC and Pt(0)/TPA@AC very attractive catalysts for performing selective dehydrocoupling reactions.

Acknowledgements

The authors would like to thank Dumlupinar University BAP (2015-50) for the financial support. The partial support by the Science Academy is gratefully acknowledged.

Notes and references

- 1 Basic Research Needs For the Hydrogen Economy, Report of the Basic Energy Sciences Workshop on Hydrogen Production, Storage and Use, 2003, Office of Science, U. S. Department of Energy, May 13–15.
- 2 M. Gulcan, M. Zahmakiran and S. Özkar, *Appl. Catal., B*, 2014, **147**, 394–401.
- 3 Annual Energy Outlook 2005 With Projections To 2025, Energy Information Administration, February 2005.
- 4 J. Turner, G. Sverdrup, K. Mann, P. G. Maness, B. Kroposki, M. Ghirardi, R. J. Evans and D. Blake, *Int. J. Energy Res.*, 2007, **32**, 379.
- 5 IAC Report, *Lighting the Way Towards a Sustainable Energy Futures*, Interacademy Council, Amsterdam, 2007.
- 6 W. Grochala and P. P. Edwards, *Chem. Rev.*, 2004, **104**, 1283.
- 7 P. Chen, Z. T. Xiong, J. Z. Luo, J. Y. Lin and K. L. Tan, *Nature*, 2002, **420**, 302.
- 8 R. Bacsa, C. Laurent, R. Morishima, H. Suzuki and M. Lelay, *J. Phys. Chem. B*, 2004, **108**, 12718.
- 9 S. H. Lim, J. Luo, Z. Zhong, W. Ji and J. Lin, *Inorg. Chem.*, 2005, **44**, 4124.
- 10 J. A. Rood, B. C. Noll and K. W. Henderson, *Inorg. Chem.*, 2006, **45**, 5521.
- 11 Basic Research Needs Catalysis for Energy, Report from the US Department of Energy, Basic Energy Sciences Workshop Report, 2007, August 6–8.
- 12 J. Wang, S. Wasmus and R. F. Savinell, *J. Electrochem. Soc.*, 1995, **142**, 4218.
- 13 C. A. Jaska, K. Temple, A. J. Lough and I. Manners, *J. Am. Chem. Soc.*, 2003, **125**, 9424–9434.
- 14 A. Friederich, M. Drees and S. Schneider, *Chem. – Eur. J.*, 2009, **15**, 10339–10342.
- 15 C. A. Jaska and I. Manners, *J. Am. Chem. Soc.*, 2004, **126**, 9776–9785.
- 16 Y. Chen, J. L. Fulton, J. C. Linehan and T. Autrey, *Prepr. Pap. – Am. Chem. Soc., Div. Fuel Chem.*, 2004, **49**, 972–973.
- 17 Y. Chen, J. L. Fulton, J. C. Linehan and T. Autrey, *J. Am. Chem. Soc.*, 2005, **127**, 3254–3255.
- 18 T. J. Clark, C. A. Russell and I. Manners, *J. Am. Chem. Soc.*, 2006, **128**, 9582–9583.
- 19 M. E. Sloan, A. Staubitz, T. J. Clark, C. A. Russell, G. C. Lloyd-Jones and I. Manners, *J. Am. Chem. Soc.*, 2010, **132**, 3831–3841.
- 20 G. Alcaraz, L. Vendier, E. Clot and S. Sabo-Etienne, *Angew. Chem., Int. Ed.*, 2010, **49**, 918–920.
- 21 F. Durap, M. Zahmakiran and S. Özkar, *Appl. Catal., A*, 2009, **369**, 53–59.
- 22 M. Zahmakiran and S. Özkar, *Inorg. Chem.*, 2009, **48**, 8955–8964.
- 23 M. Zahmakiran, M. Tristany, K. Philippot, K. Fajerweg, S. Özkar and B. Chaudret, *Chem. Commun.*, 2010, **46**, 2938–2940.
- 24 Y. Jiang and H. Berke, *Chem. Commun.*, 2007, 3571–3573.
- 25 J. L. Fulton, J. C. Linehan, T. Autrey, M. Balasubramanian, Y. Chen and N. K. Szymczak, *J. Am. Chem. Soc.*, 2007, **129**, 11936–11949.
- 26 M. E. Sloan, T. J. Clark and I. Manners, *Inorg. Chem.*, 2009, **48**, 2429–2435.
- 27 M. Yurderi, A. Bulut, M. Zahmakiran, M. Gulcan and S. Özkar, *Appl. Catal., B*, 2014, **160–161**, 534–541.
- 28 M. Munoz-Olasagasti, A. Telleria, J. Perez-Miqueo, M. A. Garralda and Z. A. Freixa, *Dalton Trans.*, 2014, **43**, 11404–11409.
- 29 F. Sen, Y. Karatas, M. Gulcan and M. Zahmakiran, *RSC Adv.*, 2014, **4**, 1526–1531.
- 30 D. Pun, E. Lobkovsky and P. J. Chirik, *Chem. Commun.*, 2007, 3297.
- 31 (a) Z. Liu, X. Y. Ling, X. Su and J. Y. Lee, *J. Phys. Chem. B*, 2004, **108**, 8234–8240; (b) F. Sen, S. Sen and G. Gökağaç, *Phys. Chem. Chem. Phys.*, 2011, **13**, 1676; (c) F. Sen and G. Gökağaç, *J. Appl. Electrochem.*, 2014, **44**, 199; (d) S. Sen, F. Sen and G. Gökağaç, *Phys. Chem. Chem. Phys.*, 2011, **13**, 6784; (e) F. Sen and G. Gökağaç, *J. Phys. Chem. C*, 2007, **111**, 1467.
- 32 H. Klug and L. Alexander, *X-ray diffraction procedures*, Wiley, New York, 1st edn, 1954.

- 33 (a) T. Yonezawa, N. Toshima, C. Wakai, M. Nakahara, M. Nishinaka, T. Tominaga and H. Nomura, *Colloids Surf., A*, 2000, **169**, 35–45; (b) H. Pamuk, B. Aday, F. Şen and M. Kaya, *RSC Adv.*, 2015, **5**, 49295; (c) F. Şen and G. Gökağaç, *Energy Fuels*, 2008, **22**, 1858–1864; (d) Z. Ozturk, F. Sen, S. Sen and G. Gokagac, *J. Mater. Sci.*, 2012, **47**, 8134–8144.
- 34 F. Sen and G. Gökağaç, *J. Phys. Chem. C*, 2007, **111**, 5715–5720.
- 35 P. T. A. Sumodjo, E. J. Silva and T. Rabochai, *J. Electroanal. Chem.*, 1989, **271**, 305.
- 36 S. Ertan, F. Sen, S. Sen and G. Gökağaç, *J. Nanopart. Res.*, 2012, **14**, 922.
- 37 F. Sen, G. Gökağaç and S. Sen, *J. Nanopart. Res.*, 2013, **15**, 1979.
- 38 T. C. Deivaraj, W. X. Chen and J. Y. Lee, *J. Mater. Chem.*, 2003, **13**, 2555.
- 39 S. Özkar and R. G. Finke, *J. Am. Chem. Soc.*, 2002, **124**, 5796.
- 40 K. J. Laidler, *Chemical Kinetics*, Benjamin-Cummings, UK, 3rd edn, 1997.
- 41 H. Eyring, *J. Chem. Phys.*, 1935, **3**, 107.
- 42 Y. Sun, L. Zhuang, J. Lu, X. Hong and P. Liu, *J. Am. Chem. Soc.*, 2007, **129**, 15465.
- 43 Y. Kawano, M. Uruichi, M. Shiomi, S. Taki, T. Kawaguchi, T. Kakizawa and H. Ogino, *J. Am. Chem. Soc.*, 2009, **131**, 14946.
- 44 R. J. Keaton, J. M. Blacquiere and R. T. Baker, *J. Am. Chem. Soc.*, 2007, **129**, 11936.
- 45 A. P. M. Robertson, R. Suter, L. Chabanne, G. R. Whittel and I. Manners, *Inorg. Chem.*, 2011, **50**, 12680.
- 46 E. Erken, H. Pamuk, Ö. Karatepe, G. Başkaya, H. Sert, O. M. Kalfa and F. Şen, *J. Cluster Sci.*, 2015, DOI: 10.1007/s10876-015-0892-8.